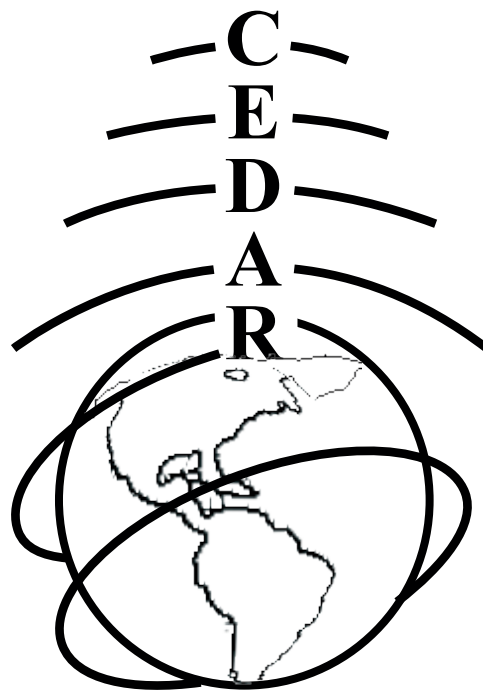


2005 Joint CEDAR-GEM Workshop
Eldorado Hotel and La Fonda Hotel
Santa Fe, New Mexico, USA
June 26 - July 1, 2005



Monday CEDAR Poster Session Booklet
June 27



Contents

1	Mesosphere-Lower Thermosphere General Studies	5
1.1	MLT.01: Forcing of the Mesospheric Semi-Annual Oscillation in the Whole Atmosphere Community Climate Model – by Beres, Jadwiga	5
1.2	MLT.02: Probing the polar mesosphere with ground-based spectroscopy of carbon monoxide – by Burrows, Susannah	5
1.3	MLT.03: Turbulent Kinetic Energy Dissipation Rates in the Tropical Mesosphere Using 2002-2004 Jicamarca Radar Data – by Guo, Liyu	5
1.4	MLT.04: Polar lower thermospheric wind dynamics based on EISCAT 8-day window data obtained in November 2003 (2): Comparison with TIME-GCM, and relative importance of ion-drag forcing. – by Nozawa, Satonori	6
1.5	MLT.05: Methodology for estimation of the lower thermospheric wind with the incoherent-scatter radar – by Oyama, Shin-ichiro	6
1.6	MLT.06: A study of the lower thermospheric wind in the polar cap on the basis of ESR data for summer days – by Tsuda, Takuo	7
1.7	MLT.07: Characteristics of Waves in the Upper Mesosphere from Ground-Based Airglow Measurements in the Northern High-Latitude – by Won, Young-In	7
1.8	MLT.08: Ground-Based Measurements of the Annual and Semi-Annual Oscillations in Mesospheric Temperatures at Low Latitudes – by Zhao, Yucheng	7
1.9	MLT.09: Height estimation of OH airglow layer via ground-based all-sky imagers – by Gobbi, Delano	8
2	Instruments and Techniques for the Middle Atmosphere	9
2.1	IATM.01: Rotational temperatures of OH(6-2) using a Temperature Imaging Spectrometer (TIS) – by Bageston, Jose presented by Gobbi, Delano	9
2.2	IATM.02: Current status of the ALOMAR Weber sodium lidar transmitter – by Acott, P	9
2.3	IATM.03: A method of wind field measurement to avoid bird’s influence with multiple-receiver UHF radar – by Chen, Meng-Yuan	10
2.4	IATM.04: Detection of Radio Meteor – by Kang, Chunmei	10
2.5	IATM.05: Radar Acquisition System at Jicamarca using off-the-shelf Digital Receivers – by Reyes, Pablo presented by Reyes, Pablo	10
2.6	IATM.06: The O(1S- ζ 1D,1P) Line Intensity Ratio – by Slanger, Tom presented by Sharpee, Brian	11
2.7	IATM.07: First Results of Upper Mesospheric and Lower Thermospheric Winds Using Fabry-Perot Interferometer at Daytona Beach, FL – by Won, Y-I presented by Azeem, Irfan	11
2.8	IATM.08: CSU sodium lidar basics: measurement principles, operation and capability – by Yue, Jia	12
3	Gravity Wave Studies	13
3.1	GWV.01: The wave-induced non-periodic response of minor species in the MLT region – by Abdo, Kevin	13
3.2	GWV.02: Correlative measurements of atmospheric gravity wave vertical wavelength using photometer phase information and sodium resonance lidar measurements – by Carlson, Chad	13
3.3	GWV.03: Observation of Mesospheric Bores in the Equatorial MLT Region – by Fechine, Joaquim	13
3.4	GWV.04: Investigation of the Temperature Inversion Layer Observed in the MLT Region During the ALOHA-93 Campaign – by Hanner, Bonnie	14
3.5	GWV.05: The mystery of gravity waves: a beginners view – by Harrell, Sean	14
3.6	GWV.06: The secular variations of OH nightglow emission induced by gravity wave forcing – by Hoang, Thien	14
3.7	GWV.07: A Numerical Model to Investigate the Propagation, Dissipation and Effects of Atmospheric Acoustic-Gravity Waves in Planetary Atmospheres – by Khanal, Harihar presented by Khanal, Harihar	15

3.8	GWV.08: Realistic Doppler Ducting of Mesospheric Gravity Waves – by Snively, Jonathan	15
3.9	GWV.09: Winter mesospheric temperature inversion and tidal-gravity wave interactions – by Li, Tao	16
3.10	GWV.10: Climatology of Small-Scale Mesospheric Gravity Waves Observed over Antarctica – by Nielsen, Kim	16
3.11	GWV.11: A curved gravity wave in the mesospheric airglow images – by Suzuki, Shin	17
3.12	GWV.12: Gravity Waves Activity over Brazil Inferred from CHAMP GPS-RO Temperature Profiles – by Wrasse, Cristiano	17
3.13	GWV.13: The sodium signature of an overturning gravity wave – by Xu, Jiyao presented by Smith, Anne	18
3.14	GWV.14: Numerical Simulations of Upward Propagating Gravity Waves in the Middle Atmosphere – by Yu, Yonghui	18
3.15	GWV.15: Evolution of a Mesospheric Bore Wave using 2D Local Spectral Analysis – by Stockwell, R.	18
4	Other Wave Studies	20
4.1	OWV.01: Planetary Wave Calculations using the Global Scale Wave Model (GSWM) – by Stockwell, R.	20
4.2	OWV.02: The 8-Hour Tide in the Mesosphere and Lower Thermosphere over the UK, 1988 - 2004 – by Beldon, Charlotte	20
4.3	OWV.03: Arctic mesopause region dynamics during the Stratospheric Polar Vortex season – by Bhattacharya, Yajnavalkya	20
4.4	OWV.04: Mean Structure and Variability of the Diurnal Tide in the NCAR Whole Atmosphere Community Climate Model – by Chang, Loren	20
4.5	OWV.05: Observations of Lunar Tides in the Mesosphere and Lower Thermosphere at Arctic and Middle Latitudes – by Sandford, David	21
4.6	OWV.06: A Climatology of Tidal Temperatures from TIMED/SABER – by Zhang, Xiaoli presented by Zhang, Xiaoli	22
5	Lidar Studies	23
5.1	LID.01: Lidar Observations of Gravity Wave Spectra at Arecibo – by Hassiotis, Alexander	23
5.2	LID.02: Comparison of Meteor Radar Wind Measurements at Barrow and Dixon Island – by Imura, Hiroyuki	23
5.3	LID.03: Observations and Modeling of Mesospheric Potassium Layer over the Arecibo Observatory – by Ruben, Delgado	23
5.4	LID.04: Analysis of Wind Speed and Wind Shear Statistics and Small Scale Structure using Doppler Lidar Data from New Mexico and Hawaii – by Zhou, Xiaoqian	24
6	Stratosphere Studies and Below	25
6.1	SSB.01: Polar stratospheric clouds observed by a lidar at Rothera, Antarctica – by Simpson, Shawn	25
6.2	SSB.02: Study of the Temperature Structure of the Middle Arctic Atmosphere – by Thuraiajah, Brentha	25
7	Sprite and Terrestrial Gamma-ray Flash (TGF) Studies	26
7.1	SPR.01: On the OH nightglow emission at Sprite temperatures in the MLT region – by Fritz, Jason	26
7.2	SPR.02: Testing Sprite Initiation Theories Using Lightning Measurements and Modeled EM Fields – by Hu, Wenyi presented by Hu, Wenyi	26
7.3	SPR.03: Using WWLLN to provide insight on Terrestrial Gamma Ray Flashes – by Lay, Erin	26
7.4	SPR.04: Comparison of Results from Sprite Streamer Modeling with Spectrophotometric Measurements by ISUAL Instrument on FORMOSAT-2 Satellite – by Liu, Ningyu presented by Liu, Ningyu	27

7.5	SPR.05: Lightning-driven electric and magnetic fields measured in the stratosphere during the Brazil 2002-03 Balloon Campaign – by Thomas, Jeremy	27
7.6	SPR.06: 3D FDTD MODELING OF THE DIURNAL AND SEASONAL VARIATIONS IN SCHUMANN RESONANCE PARAMETERS – by Yang, Heng	28
8	Coupling the Upper and Lower Atmosphere	30
8.1	CUL.01: DUMBO and the Ionosphere – by Livneh, Dorey	30
8.2	CUL.02: An Improved Approach for Atmosphere Data Analysis – by Zhang, Junbo presented by Zhou, Qihou	30
9	Meteor Science other than Winds	31
9.1	MET.01: Aeronomic Implications of Recent Arecibo UHF Meteor Observations – by Briczinski, S	31
9.2	MET.02: Calibration Issues in Meteor Radar Interferometers – by de la Pena, Santiago . . .	31
9.3	MET.03: Mysteries of the MU - Initial Observations and Analysis of MU Meteor Data – by Malhotra, Akshay	31
9.4	MET.04: Reconstructing classical meteor trail echoes a post-modern view – by Roy, Arnab	32

1 Mesosphere-Lower Thermosphere General Studies

1.1 MLT.01: Forcing of the Mesospheric Semi-Annual Oscillation in the Whole Atmosphere Community Climate Model – by Beres, Jadwiga

Status of First Author: Nonstudent

Authors: Jadwiga H. Beres (beres@ucar.edu) and R. R. Garcia (rgarcia@ucar.edu), NCAR, Boulder, CO
Abstract: The mesospheric semi-annual oscillation (MSAO) of the zonal winds is a prominent feature of the tropical atmosphere. The MSAO is out of phase with the underlying stratospheric semi-annual oscillation (SAO) and is believed to be forced by selective transmission of gravity waves and Kelvin waves propagating from the troposphere. Using NCAR's Whole Atmosphere Community Climate Model, we show that the MSAO can be forced by a combination of planetary waves and gravity waves, as well as by meridional advection. The forcing of the MSAO by planetary waves is strongest in January, when the 2-day wave amplitudes are the largest.

1.2 MLT.02: Probing the polar mesosphere with ground-based spectroscopy of carbon monoxide – by Burrows, Susannah

Status of First Author: CEDAR student in the poster competition Undergraduate

Authors: Susannah Burrows, Oberlin College, susannah.burrows@oberlin.edu Christopher L. Martin, Oberlin College, chris.martin@oberlin.edu

Abstract: The mesospheric region, where much of the important energy transfer in the Earth's atmosphere takes place, is difficult to measure with most remote sensing techniques, as it is too high for balloon measurements and yet lower than the reach of aurora and meteor radar studies. Radiometric measurements of carbon monoxide (CO), which reaches its highest density in the middle atmosphere, present a particularly convenient method of obtaining information about this region. Until recently, most continuous measurements of atmospheric CO have been obtained by mid-latitude ground observations of the $J = 1 - 0$ rotational transition. The Antarctic Sub-millimeter Telescope/Remote Observatory is capable of observing the $J = 2-1$, $J = 4-3$, and $J = 7-6$ rotational transitions of CO and thus can see CO emission spectra from the upper mesosphere and lower thermosphere, between about 40 and 130 km. Mesospheric wind velocity data and density and mixing profile results obtained from curve fitting to CO profiles will be presented.

1.3 MLT.03: Turbulent Kinetic Energy Dissipation Rates in the Tropical Mesosphere Using 2002-2004 Jicamarca Radar Data – by Guo, Liyu

Status of First Author: CEDAR student in the poster competition Masters

Authors: L. Guo (lguo@clemson.edu, Clemson Univ.), G. Lehmac (glehmac@CLEMSON.EDU, Clemson Univ.) E. Kudeki (erhan@uiuc.edu, UIUC), R. Sheth (UIUC), J. Chau (jchau@jro.igp.gob.pe, JRO) M. Milla (mmilla@uiuc.edu, UIUC) P. Reyes (preyes@jro.igp.gob.pe, JRO)

Abstract: The MST radar at Jicamarca Radar Observatory (JRO) is a powerful radar that can detect atmospheric turbulence on the Bragg scale of 3m in the Mesosphere 60-85km altitude region. The spectral widths calculated from the spectrum for days in March 2003, May 2003 and July 2002, 2004 have been used to compute the kinetic energy dissipation rates D and eddy diffusivity K due to atmospheric turbulence following the method by Weinstock [1981]. The contamination due to beam broadening caused by a small beamwidth of 0.7 deg has been removed. The daily median D and K as well as the monthly median D and K are calculated. Comparisons with the similar studies at other geographic locations are made. K and D increase with height which is consistent with the result of Fukao et al. [1994].

1.4 MLT.04: Polar lower thermospheric wind dynamics based on EISCAT 8-day window data obtained in November 2003 (2): Comparison with TIME-GCM, and relative importance of ion-drag forcing. – by Nozawa, Satonori

Status of First Author: Nonstudent

Authors: S. Nozawa (STEL, Nagoya University, nozawa@stelab.nagoya-u.ac.jp) A. Brekke (University of Tromsø, Asgeir.Brekke@phys.uit.no) S. Maeda (Kyoto women's University, smaeda@kyoto-wu.ac.jp) T. Aso (National Institute Polar Research, t-aso@nipr.ac.jp) C. M. Hall (University of Tromsø, Chris.Hall@tgo.uit.no) Y. Ogawa (STEL, Nagoya University, yogawa@stelab.nagoya-u.ac.jp) S. C. Buchert (Swedish Institute of Space Physics, scb@irfu.se) J. Roettger (National Institute Polar Research, roettger@linmpi.mpg.de) A. D. Richmond (NCAR High Altitude Observatory, richmond@ucar.edu) R. Roble (NCAR High Altitude Observatory, roble@ucar.edu) and R. Fujii rfujii@stelab.nagoya-u.ac.jp

Abstract: Simultaneous Incoherent Scatter radar observations using two EISCAT radars, the Tromsø (69.6 degree N, 19.2 degree E) UHF radar and the EISCAT Svalbard radar (Longyearbyen 78.2 degree N, 16.0 degree E) were conducted for eight consecutive days, from November 11 to 19, 2003, to study the lower thermospheric wind dynamics in the polar region. Derived wind data were analyzed, in particular, in terms of the latitudinal difference of the mean wind and diurnal and semidiurnal tides as well as the presence of the quasi-two day wave (Q2DW) in the lower thermosphere. In this presentation, we mainly focus on two topics such as relative importance of ion-drag forcing as well as comparison of the derived wind with NCAR TIME-GCM predictions. Ion-drag acceleration of the wind is generally negligible below 107 km at Tromsø and below 118 km at Longyearbyen, but significant ion-drag acceleration is found above these heights. A comparison of mean wind and tidal amplitudes and phases with NCAR Thermosphere-Ionosphere-Mesosphere-Electrodynamics general circulation model (TIME-GCM) predictions for the period shows some agreement, but the model semidiurnal amplitude is too small, and the vertical wavelength is too large, in comparison with the observations.

1.5 MLT.05: Methodology for estimation of the lower thermospheric wind with the incoherent-scatter radar – by Oyama, Shin-ichiro

Status of First Author: Nonstudent

Authors: S. Oyama: Geophysical Institute, University of Alaska Fairbanks, USA, soyama@gi.alaska.edu B. J. Watkins: Geophysical Institute, University of Alaska Fairbanks, USA, bjw4072@mailblocks.com S. Maeda: Kyoto Women's University, Japan, smaeda@kyoto-wu.ac.jp S. Nozawa: Solar-Terrestrial Environment Laboratory, Nagoya University, Japan, nozawa@stelab.nagoya-u.ac.jp C. Lathuillere, Laboratoire de Planetologie de Grenoble, France, Chantal.Lathuillere@obs.ujf-grenoble.fr W. Kofman, Laboratoire de Planetologie de Grenoble, France, wlodek.kofman@obs.ujf-grenoble.fr

Abstract: The coupled mesosphere-thermosphere-ionosphere system at high latitudes exhibits complicated temporal and spatial variations in association with the energy coupling between upper and lower regions. While our knowledge of this system has been extended during the last three decades, various interesting phenomena remain to be known in that region. One of them is the lower thermospheric wind dynamics in association with geomagnetic activity. To progress our understanding in this field, our group has conducted variety experiments with the Sondrestrom incoherent-scatter (IS) radar and the European Incoherent Scatter (EISCAT) radar since 2003. The presentation addresses the methodology for estimation of lower thermospheric winds, which is developed to optimize the neutral wind estimation with the monostatic or beam-swinging methods and the tristatic method using the KST (Kiruna-Sodankyla-Tromsø) UHF radar. In particular, the developed method has a vantage point to estimate the vertical component of neutral wind velocity. The presentation also show some results of the wind dynamics from these experiments during disturbed periods.

1.6 MLT.06: A study of the lower thermospheric wind in the polar cap on the basis of ESR data for summer days – by Tsuda, Takuo

Status of First Author: CEDAR student in the poster competition PhD

Authors: T. Tsuda, S. Nozawa, Y. Ogawa, and R. Fujii, Solar-Terrestrial Environment Laboratory, Nagoya University, Japan. (e-mail: ttsuda@stelab.nagoya-u.ac.jp; nozawa@stelab.nagoya-u.ac.jp; yogawa@stelab.nagoya-u.ac.jp; rfujii@stelab.nagoya-u.ac.jp) A. Brekke, Faculty of science, University of Troms, Norway. (e-mail:Asgeir.Brekke@phys.uit.no)

Abstract: On the basis of data obtained by the EISCAT Svalbard Radar (ESR) located at Longyearbyen (78.2 deg N, 16.0 deg E), we have studied the lower thermospheric wind dynamics in the polar cap. Two CP-2 datasets obtained for 1-9 July 1999 (higher solar activity) and 4-14 June 2004 (lower solar activity) were analyzed in order to understand characteristics of mean winds, tides and quasi-2 day wave (Q2DW) in the lower thermosphere in the polar cap. Results are summarized as follows: In general, similar features are found for the mean winds and the diurnal tidal components between the two intervals. The meridional mean wind blew northward, while the zonal mean wind changed the direction from east to west with increasing altitude. The diurnal tidal amplitudes increased with altitude increasing, and the diurnal tide became mainly the largest wave component above 110 km. For the semidiurnal tide and the Q2DW, different features between the two datasets are found. The semidiurnal amplitude in the meridional and zonal components maximized at 105-110 km with values of 40-50 m s⁻¹ for 4-14 June 2004. In contrast, the zonal semidiurnal tidal amplitude was very weak for 1-9 July 1999. Concerning the Q2DW, it was observed with amplitude of 20-30 m s⁻¹ above 110 km for 1-3 July 1999, while it was not observed for 4-14 June 2004. Furthermore, we compared ion-drag, Coriolis and total accelerations. Relative importance of the ion-drag acceleration was growing with altitude increasing for both intervals.

1.7 MLT.07: Characteristics of Waves in the Upper Mesosphere from Ground-Based Airglow Measurements in the Northern High-Latitude – by Won, Young-In

Status of First Author: Nonstudent

Authors: Young-In Won, G. G. Sivjee, S. M. I. Azeem, Department of Physical Science, Embry-Riddle Aeronautical University won408@erau.edu
Q. Wu HAO/NCAR

Abstract: Terrestrial nightglow emissions in the near infrared region have been monitored from two ground-based optical observatories in the northern high latitude; Eureka (80.0N, 85.9 W), and Resolute Bay (74.68 N, 94.90 W), Canada. We have used rotational temperature and wind information derived from Michelson Interferometer and Fabry-Perot Interferometer observations of OH Meinel bands to study the periodicities of the atmospheric waves that are known to propagate upward from the lower atmosphere and perturb the upper mesospheric region. The sliding Lomb-Scargle analysis shows various spectral peaks near tidal periods. The commonly observed features are waves near the tidal periods, i.e. 6, 8, and 12 hour oscillations. Harmonic analysis is also performed to identify the amplitudes and phase information of the major oscillations over season.

1.8 MLT.08: Ground-Based Measurements of the Annual and Semi-Annual Oscillations in Mesospheric Temperatures at Low Latitudes – by Zhao, Yucheng

Status of First Author: Nonstudent

Authors: Yucheng Zhao Utah State University yucheng@cc.usu.edu
Mike J. Taylor Utah State University mtaylor@cc.usu.edu
Hanli Liu HAO, NCAR liuh@ucar.edu
Ray Roble HAO, NCAR Roble@ucar.edu

Abstract: Long term measurements of the near IR mesospheric OH and O2 emissions have been made from Haleakala Crater, Maui, Hawaii (20.8N, 156.2W) as part of the Maui-MALT program. Observations have been made routinely since October 2001 (typically 22 days/month) using the CEDAR Mesospheric Temperature Mapper (MTM). This imager sequentially measures the OH (6, 2) band intensity and temperature (peak altitude 87km) and the O2 (0, 1) Atmospheric band intensity and temperature (peak altitude 94km) with a precision of 1-2 K in 3 minutes. Over 600 nights of quality data (durations typically 4-10 hours) have been obtained to date. Detailed analysis revealed significant nocturnal and seasonal variability. In particular, the semi-annual oscillation (SAO) is evident in mesospheric temperature with peaks occurring during the Spring and Fall in good agreement with the well established SAO signatures in the mesospheric wind field. In this analysis, we investigate the amplitude and phase of SAO and the contribution of the annual oscillation (AO) at this low-latitude site. With three year of data, the intra-annual variability is also investigated.

1.9 MLT.09: Height estimation of OH airglow layer via ground-based all-sky imagers – by Gobbi, Delano

Status of First Author: Nonstudent PhD

Authors: Delano Gobbi, INPE, Brazil Paulo R. Fagundes, UNIVAP, Brazil Valdir G. Pillat, UNIVAP, Brazil Hisao Takahashi, INPE, Brazil Fabio A. Vargas, INPE, Brazil Cristiano M. Wrasse, INPE, Brazil Jose R. Abalde, UNIVAP, Brazil

Abstract: This work presents the results concern to the height estimation of OH airglow layer by using simultaneous images observed at two distinct sites, Cachoeira Paulista Observatory (22.70 S) and Brasopolis Observatory (23.50 S). The height of airglow structure is determined by analysis of the optimum cross-correlation coefficient between two wave events, with horizontal scales in the range of 10-150 km, seen in the respective imagers (Kubota et al, 1999). This study provides a preliminary characterization on the variability of the OH airglow vertical structure at brazilian sites.

2 Instruments and Techniques for the Middle Atmosphere

2.1 IATM.01: Rotational temperatures of OH(6-2) using a Temperature Imaging Spectrometer (TIS) – by Bageston, Jose presented by Gobbi, Delano

Status of First Author: Student NOT in the poster competition Masters

Authors: Jose V. Bageston, INPE, Brazil Delano Gobbi, INPE, Brazil Hisao Takahashi, INPE, Brazil Cristiano M. Wrasse, INPE, Brazil

Abstract: This work shows a recent Temperature Imaging Spectrometer (TIS) designed and constructed at INPE in order to observe the rotational temperature of OH(6-2) Meinel band. It is aimed to monitor the mesopause temperature with a high precision (± 2 K) and stability for long-term observation. The methodology to derive the rotational temperature is described in details and some results are discussed. The TIS consist of a cooled CCD camera with 1024 x 1024 pixel and a telecentric lens system (field-of-view 200) in order to get a spatially homogeneous, but frequency dispersed image. The images data are 2 x 2 binned to get a better signal-noise ratio. The OH(6-2) P-branch spectrum forms a ring pattern on the image plain, each fringe relating to P1(4), P1(3) and P1(2) rotational lines. Therefore, the rotational temperature was calculated from the P1(4)/P1(2) line intensity ratio. The preliminary results obtained at Cachoeira Paulista (22.7 S, 45.0 W), Brazil, will be presented.

2.2 IATM.02: Current status of the ALOMAR Weber sodium lidar transmitter – by Acott, P

Status of First Author: CEDAR student in the poster competition PhD

Authors: Acott(acott@lamar.colostate.edu) Williams(biffw@lamar.colostate.edu), Vance(citruslaser@gmail.com), Yue(jyue@lamar.colostate.edu), Harrell(sharrel@lamar.colostate.edu), She(joeshe@lamar.colostate.edu)

Abstract: ALOMAR (Arctic Lidar Observatory for Middle Atmospheric Research) is an international facility devoted to multi-instrument research of the earth's middle atmosphere. In addition to several lidar systems covering from the troposphere to the lower thermosphere, there are MF, meteor, and MST radars, a rocket launch facility, and infrared and auroral imagers. A recent joint lidar-rocket-radar campaign devoted to the study of the polar summer mesosphere produced 7 high quality papers featured as the cover in a special December 28, 2004, issue of Geophysics Research Letters (GRL). Our lidar data showing a temperature gradient with latitude of 40 K/km and a photograph of our dual laser beams are inserts on the cover.

The ALOMAR-Weber sodium lidar, located within the Arctic Circle in Andenes, Norway, uses an innovative Sum Frequency Generation (SFG) method to generate the continuous light at 589nm to seed the pulse transmitter of the lidar for simultaneous temperature, horizontal wind, and sodium density measurements in the mesopause region (80-110Km). After many successful campaigns, the unique SFG resonator experienced a coating failure. This coating failure caused other problems, in addition to just replacing the resonator, including system re-alignment and optimization. Since installation of a nitrogen purge and changing from a plasma coating to a harder ion-beam-sputtered (IBS) coating in April 2004, there has been no trace of resonator failure and thus no need for re-alignment and optimization. This poster will present the current status ALOMAR Weber lidar system including: its stable and robust operation, the ability to monitor and help operate the system remotely from Fort Collins over the internet, and the training of and operation by our highly motivated and talented colleagues in Norway. In addition to the current system a low-power SFG for measuring the Faraday filter spectrum is being developed in Fort Collins for later deployment at ALOMAR.

We will present data from the recent Dec 2004 DELTA rocket campaign showing a wave perturbing a background temperature profile with a near adiabatic lapse rate, resulting in multiple adiabatic layers.

2.3 IATM.03: A method of wind field measurement to avoid bird's influence with multiple-receiver UHF radar – by Chen, Meng-Yuan

Status of First Author: CEDAR student in the poster competition PhD

Authors: Meng-Yuan Chen Institute of Space Science, National Central University, Taiwan.
s1643009@cc.ncu.edu.tw

Tian-You Yu School of Electrical and Computer Engineering, University of Oklahoma, Norman, Oklahoma, USA tyu@ou.edu

Yen-Hsyang Chu Institute of Space Science, National Central University, Taiwan
yhchu@jupiter.ss.ncu.edu.tw

Abstract: Atmospheric radar is a powerful instrument for study of the structure and dynamics of the atmosphere. Unfortunately, it sometimes receives unexpected signals besides atmospheric echo. In this work, a post process is applied to measure the wind field and avoid the influence of a bird. This method is described theoretically from a view of radar imaging. It probably works if a weighting function, which has potential to reduce interfering signal is chosen. Simulations based on multiple antenna profiler radar (MAPR) have been implemented to verify this method. The results show that it is superior to avoid strong interference from a point target. Then apply this method to the observation data of MAPR to demonstrate it's advantage. Although this work is focus on the UHF band, it also can be used for other frequencies.

2.4 IATM.04: Detection of Radio Meteor – by Kang, Chunmei

Status of First Author: CEDAR student in the poster competition PhD

Authors: Chunmei Kang, Aerospace Engineering Sciences department, Colorado University, chunmei.kang@colorado.edu Scott E Palo, Assistant Professor, Aerospace Engineering Sciences Department, University of Colorado, palo@colorado.edu,

Abstract: Underdense meteor echoes observed using very high frequency (VHF) radar can be accurately modeled as a single complex damped sinusoid in additive white Gaussian noise. The damping coefficient is expected to be between 0 and 0.6 for a VHF meteor return based on the modeled ambipolar diffusion rates near 90km. Current meteor echo detection routines operate either in the frequency domain, when it is difficult to detect highly damped signals, or in the time domain, where it is difficult to detect narrow band signals. An added difficulty is that many of these approaches require a priori knowledge of the noise variance. In this paper, a time-frequency waveform detector is proposed to solve this problem. By normalizing the power and power spectral density of a signal in the time and frequency domains respectively, and the detector is invariant to the noise variance. The waveform difference of a damped sinusoid in the time and frequency domain is used to detect a damped signal in noise. The proposed detector is only a function of the number of samples and is stable with various damping coefficients and noise levels. Compared with the conventional energy detector or power detector, the time-frequency waveform detector exhibits better detection probability for highly damped signals when the noise variance is unknown. We present numerical results that demonstrate the effectiveness of this detector.

2.5 IATM.05: Radar Acquisition System at Jicamarca using off-the-shelf Digital Receivers – by Reyes, Pablo presented by Reyes, Pablo

Status of First Author: Student NOT in the poster competition Undergraduate

Authors: Pablo Reyes(preyes@jro.igp.gob.pe) Karim Kuyeng(kkuyeng@jro.igp.gob.pe) Darwin Cordova(dcordova@jro.igp.gob.pe) Gabriel Michhue(gmichhue@jro.igp.gob.pe) F. Villanueva(fvillanueva@jro.igp.gob.pe) Jorge L. Chau(jchau@jro.igp.gob.pe)
Radio Observatorio de Jicamarca Instituto Geofisico del Peru

Abstract: After more than 40 years using analog receivers at the Jicamarca Radio Observatory (JRO) and continuing with the idea to develop improved acquisition systems, we have now implemented a new system based on an off-the-shelf digital receivers, which using a common stable 10 MHz clock (GPS-controlled), gives us the opportunity to have coherence between Radar Controller, Digital Direct Synthesizer, and receiver clocks in both monostatic and bistatic configurations.

To take advantage of the digital receiving filter, recent hardware improvements have been also added to the system. For example, we have developed and implement new limiters based on Schottky Diodes. These limiters have better insertion loss as well as bandwidth, than the previous 40-year-old limiters.

In this work, we describe the different parts of the system, particularly the Digital Receiver part. We currently have a six-channel version using three two-channel Echotek cards, running on a single PC. We will show examples of the type of experiments we have already conducted, as well as our near future plans to improve the data throughput and number of receiving channels.

2.6 IATM.06: The O(1S-1D,1P) Line Intensity Ratio – by Slanger, Tom presented by Sharpee, Brian

Status of First Author: Nonstudent

Authors: T. G. Slanger, SRI International, tom.slanger@sri.com P. C. Cosby, SRI International, philip.cosby@sri.com B. D. Sharpee, SRI International, brian.sharpee@sri.com K. R. Minschwaner, New Mexico Institute of Mining and Technology, krm@kestrel.nmt.edu D. E. Siskind, Naval Research Laboratory, siskind@uap2.nrl.navy.mil

Abstract: The ratio of intensities of the two optically-forbidden emission lines, O(1S-1D) at 557.7 nm and O(1S-3P) 297.2 nm, as observed in atmospheric emission, should be a fixed quantity since both lines arise from the same upper level. The intensity ratio should therefore equal only the ratio of spontaneous emission coefficients associated with these lines. However, the actual value of this ratio is in doubt, since most recent theoretical determinations of these coefficients yield a ratio $A(557.7)/A(297.2)$ 16, but experimental determinations have consistently yielded higher values of the $I(557.7)/I(297.2)$ ratio (18-24). We have observed these emission lines in the airglow via a combination of satellite, rocket, and ground-based spectra, each separately intensity calibrated, and have arrived at a consistent value for the intensity ratio of 9, significantly lower than either the theoretical or experimental cases. We will show that the problems of inter-comparing spectra from disparate instruments observing in different wavelength regions to make this determination is circumvented by our knowledge of the relative intensities of individual O₂ Herzberg I system bands that can be used to link the two spectral regions. This is a particularly troubling problem given the magnitude of the disagreement, and because an exact determination of this ratio is needed to allow the often-observed 297.2 nm line to act as an appropriate proxy for the intensity of the often unobserved 557.7 nm line in planetary atmosphere spectra.

2.7 IATM.07: First Results of Upper Mesospheric and Lower Thermospheric Winds Using Fabry-Perot Interferometer at Daytona Beach, FL – by Won, Y-I presented by Azeem, Irfan

Status of First Author: Nonstudent

Authors: Young-In Won, S. M. I. Azeem, G. G. Sivjee Department of Physical Science, Embry-Riddle Aeronautical University 600 S. Clyde Morris Blvd., Daytona Beach, FL 32114 e-mail: won408@erau.edu; azeem71d@erau.edu; sivjee@erau.edu

Abstract: A Fabry-Perot Interferometer (FPI) has been set-up at Embry-Riddle Aeronautical University, Daytona Beach, FL. The FPI measures the Doppler profiles of the interference fringes of the light emissions from the airglow. Since the light-emitting elements (OH, OI, OII, etc.) have been shown to be in thermal equilibrium with the surrounding neutral media, and move together with this neutral background, we can derive Doppler temperatures and winds of the peak emission height from the Doppler width and the peak

wavelength of an airglow emission spectral profile. The Daytona Beach FPI measurements comprise MLT winds from three channels (5577A, 6300A, and 8920A). We show first results from this system and compare them to Horizontal Wind Model (HWM) and Vector Spherical Harmonic Model (VSH).

2.8 IATM.08: CSU sodium lidar basics: measurement principles, operation and capability – by Yue, Jia

Status of First Author: CEDAR student in the poster competition PhD

Authors: Yue (jyue@lamar.colostate.edu), Harrell (sharrell@lamar.colostate.edu), Yuan (titus@lamar.colostate.edu) Colorado State University

Abstract: CSU sodium lidar system, deployed in August 1989, has been upgraded since May 2002 to observe MLT region temperature and horizontal wind above Fort Collins, CO on 24-hour continuous basis, weather permitting. We will introduce the measurement principle and innovative devices which made these measurements possible. They include Na Doppler-free spectrograph, a Na Faraday filter, and an acousto-optic modulator, which, respectively, provides an absolute frequency marker, make possible the measurements under sunlight conditions, and temperature and line-of-sight wind simultaneously. We will also describe how the different parts of the transmitter and receiver work together automatically via computer control to produce useful photon profiles, from which mesopause region temperature, zonal and meridional wind profiles are derived from the first principle of atomic physics. This system has quantified the MLT thermal structure with cold summer and warm winter. The longest campaign ever with this lidar lasted for 9 days continuous in September 2003 with simultaneous T, U, V observations. Time series of temperature and wind contours reveal tidal period oscillations (12-hour and 24-hour) as well as shorter period gravity wave perturbations without much analysis.

3 Gravity Wave Studies

3.1 GWV.01: The wave-induced non-periodic response of minor species in the MLT region – by Abdo, Kevin

Status of First Author: CEDAR student in the poster competition Undergraduate

Authors: Kevin Abdo, Penn State University, ksa137@psu.edu Tai-Yin Huang, Penn State University, tuh4@psu.edu Michael P. Hickey

Abstract: A time evolution of minor species to dissipating gravity wave packets is simulated with a 2-dimensional, time-dependent OH chemistry model to study the gravity-wave effects on the minor species when propagating upward through the OH nightglow emission layer in the mesosphere/lower thermosphere region. Two 20 min period wave packets have been chosen with differing 30 and 60 km horizontal wavelengths. Both wave packets were launched at three latitudes in the northern hemisphere in March to investigate the latitudinal variation in this study. In addition to causing the minor species densities to fluctuate, the wave packets also cause a secular or non-periodic variation of the minor species densities as a consequence of violation of the non-acceleration conditions due to wave transience and dissipation. The associated fluxes of minor species are downward, and so consequently minor species densities typically decrease at altitudes above where peak densities occur, and increase at altitudes below where peak densities occur. The downward flux and subsequent chemical recombination of atomic oxygen is particularly important and can cause large secular variations of other less abundant minor species densities.

3.2 GWV.02: Correlative measurements of atmospheric gravity wave vertical wavelength using photometer phase information and sodium resonance lidar measurements – by Carlson, Chad

Status of First Author: CEDAR student in the poster competition PhD

Authors: Chad G. Carlson, cgcarlson@gmail.com Gary M. Swenson, swenson1@uiuc.edu Alan Z. Liu, liuzr@uiuc.edu

Abstract: The University of Illinois at Urbana-Champaign (UIUC) currently operates a three-channel high temporal resolution photometer at Maui, HI (3.5o FOV) that observes the airglow of the OH Meinel band (840 nm), one of the O₂ atmospheric bands (865 nm) and a background band at 815 nm. The photometer provides 10 second resolution data of the intensity response of the airglow layers to modulation by atmospheric gravity waves (AGWs). The OH and O₂ layers are nominally separated by a distance of 6 km and the phase difference between the layers can be used to infer vertical wavelength and phase speed. Current work has been focused on extracting this phase information from the high temporal resolution photometer data to determine vertical wavelengths of waves observed during the Maui/MALT lidar campaign during August 9-12, 2004. The lidar measurements allow Doppler correction and determination of the intrinsic frequency. Using the measured intrinsic frequency and vertical wavelength, the horizontal wavelength is determined via the dispersion relation.

3.3 GWV.03: Observation of Mesospheric Bores in the Equatorial MLT Region – by Fechine, Joaquim

Status of First Author: Student NOT in the poster competition PhD

Authors: Fechine, J. (joaquim@laser.inpe.br)¹ Medeiros, A.F. (afragoso@df.ufcg.edu.br)² Burity, R.A. (rburity@df.ufcg.edu.br)² Takahashi, H. (hisaotak@laser.inpe.br)¹ Wrasse, C.M. (cmw@laser.inpe.br)¹
 1. Instituto Nacional de Pesquisas Espaciais (INPE), Brazil
 2. Universidade Federal de Campina Grande, Brazil

Abstract: Mesospheric bore events were observed and analyzed in the equatorial region. An all-sky CCD imager designed to measure wave structure of the OH, O2b(0,1) and OI557.7 nm airglow emission layers has been operated near the equatorial region at So Joo do Cariri (Cariri), Brazil, (7.4S, 36.5W). A large number of gravity wave was observed from September 2000 to September 2002 and among them 64 wave events were identified as mesospheric bores. The bore front shows a horizontal extension larger than 1000 km, showing a complementary brilliance between the three emissions. Their predominant characteristics as well as the occurrence, local time dependency, morphology and propagation direction will be presented and discussed.

3.4 GWV.04: Investigation of the Temperature Inversion Layer Observed in the MLT Region During the ALOHA-93 Campaign – by Hanner, Bonnie

Status of First Author: CEDAR student in the poster competition Undergraduate

Authors: Bonnie Hanner, T.-Y. Huang (1) and M. P. Hickey(2)

1. Department of Physics, The Penn State University Lehigh Valley, Fogelsville, PA 18062, USA. blh209@psu.edu, tuh4@psu.edu 2. Physical Science Department, Embry-Riddle Aeronautical University, Daytona Beach, FL 32114, USA. michael.hickey@erau.edu

Abstract: A full-wave model is used to simulate the temperature inversion layer observed in the ALOHA-93 Campaign. Previous studies have indicated that tidal forcing acting alone is not energetic enough to produce a large temperature increase (40 K) in a short span of time (1-3 hours), as observed during the Campaign. The compelling candidate for producing the MILs in the MLT region seems to be gravity wave forcing coupled with tides. Previously we proposed that the MIL observed in the ALOHA-93 Campaign was formed by the breaking of a gravity wave coupling with tides as a critical-layer interaction. Our model successfully described the qualitative features of the observations. In this study, a quasi-linear full-wave model is utilized to simulate the formation of the MIL observed in the Campaign in a quantitative sense. The initial profiles of wind and temperature were directly taken from the ALOHA-93 measurements. Our model simulations are encouraging in that it captures key features of the observed MIL in the Campaign.

3.5 GWV.05: The mystery of gravity waves: a beginners view – by Harrell, Sean

Status of First Author: Student NOT in the poster competition PhD

Authors: Sean Harrell Colorado State University sharrell@lamar.colostate.edu , Jia Yue Colorado State University jyue@lamar.colostate.edu , David Krueger Colorado State University krueger@lamar.colostate.edu , Joe She Colorado State University joeshe@colostate.edu

Abstract: To most beginning students of the atmosphere, gravity waves might appear mysterious. How do they form? How do they propagate? What causes their filtering and breaking? How do they affect the temperatures of the mesosphere and lower thermosphere? How can they be detected? These are all important questions that the beginner might raise. This poster will attempt to answer those questions in a way that newcomers to gravity waves will be able to understand. Specifically, we will show how gravity waves are filtered by critical layers in the atmosphere, which helps to explain the cold summer and warm winter mesosphere. We will also show data from the Colorado State lidar with simultaneous measurements of temperature and horizontal wind, suggesting that some of our understanding of gravity waves actually represents reality.

3.6 GWV.06: The secular variations of OH nightglow emission induced by gravity wave forcing – by Hoang, Thien

Status of First Author: CEDAR student in the poster competition Undergraduate

Authors: Thien Hoang, Tai-Yin Huang (1) and Michael P. Hickey (2)

1. Department of Physics, The Penn State University Lehigh Valley, Folgersville, PA 18062, USA. tdh155@psu.edu, tuh4@psu.edu 2. Physical Science Department, Embry-Riddle Aeronautical University, Daytona Beach, FL 32114, USA. michael.hickey@erau.edu

Abstract: The secular variations of OH airglow (8,3) band and of the intensity-weighted temperature induced by a gravity wave packet in the MLT region are investigated using a 2-dimensional, time-dependent, fully nonlinear model of minor species. A net-cycled average survives due to wave transience and dissipation. The integrated volume emission rates of OH (8,3) at latitude 82 degrees north shows a 20 percent increase with a 30-km wave packet and a mere 2 percent increase with a 60-km wave packet. The intensity-weighted temperature shows a minimal decrease with a 60-km wave packet and an initial increase up to 0.2 percent then a gradual decrease for the remainder of the simulation time with a 30-km wave packet. Latitudinal variations of the induced OH nightglow are also investigated. These secular variations could oftentimes be mistaken as long-period or short-period waves in the airglow observations. Therefore, care should be taken when analyzing observation data.

3.7 GWV.07: A Numerical Model to Investigate the Propagation, Dissipation and Effects of Atmospheric Acoustic-Gravity Waves in Planetary Atmospheres – by Khanal, Harihar presented by Khanal, Harihar

Status of First Author: Nonstudent

Authors: Harihar Khanal Department of Mathematics Embry-Riddle Aeronautical University harihar.khanal@erau.edu

Michael P. Hickey Department of Physical Sciences, and College of Arts and Sciences Embry-Riddle Aeronautical University michael.hickey@erau.edu

Abstract: A new 2-D time-dependent nonlinear model of acoustic-gravity wave propagation in planetary atmospheres is presented. The model uses a numerical procedure developed for solving the basic hydrodynamic and thermodynamic equations (Navier-Stokes equations) for viscous compressible flow using the Finite Volume (FV) discretization of the partial differential equations and boundary conditions. The velocity, pressure, and temperature are coupled via the Pressure Implicit with Shifting Operators (PISO) scheme [Oliverio and Issa 2001], which reduces the computing time of the fully implicit standard iterative methods. The non-reflecting Navier-Stokes Characteristic Boundary Conditions (NSCBCs) [Poinsot and Lele 1991] are employed in the nonphysical boundaries allowing disturbances to propagate freely out of the computational domain. Some preliminary simulation results are presented and computational issues are discussed.

References: Oliveira, P. J. and Issa, R. I., An Improved PISO Algorithm for the Computation of Buoyancy-Driven Flows, Numerical Heat Transfer, Part B, 40:473-493, 2001. Poinsot, T. J. and Lele, S. K., Boundary Conditions for Direct Simulations of Compressible Viscous Flows, Journal of Computational Physics, 101, 104-129, 1992.

3.8 GWV.08: Realistic Doppler Ducting of Mesospheric Gravity Waves – by Snively, Jonathan

Status of First Author: CEDAR student in the poster competition PhD

Authors: Jonathan B. Snively (Penn State University, jbs231@psu.edu) Victor P. Pasko (Penn State University, vpasko@psu.edu) Michael J. Taylor (Utah State University, mtaylor@cc.usu.edu) Wayne K. Hocking (University of Western Ontario, whocking@uwo.ca)

Abstract: Ducted atmospheric gravity waves are frequently observed in airglow imaging experiments and are known to propagate in ducts formed by thermal variations [e.g., Walterscheid et al., JASTP, 61, 461, 1999; Hecht et al., JGR, 106, 5181, 2001] and wind structure [e.g., Isler et al., JGR, 102(D22), 26301, 1997]. While gravity wave thermal ducts tend to be long-lived features of the atmosphere, Doppler ducts

arise from the wind flow associated with large-scale atmospheric wave and tidal motions. If the wave forming the Doppler duct is sufficiently large-scale and slowly-varying, it may be accurately treated as static with respect to small scale gravity waves ducted upon it [e.g., Isler et al., 1997]. Alternatively, for Doppler ducts exhibiting stronger time or spatial dependence, the effects of the duct dynamics become increasingly relevant to the propagation of the superimposed ducted waves. We here examine and compare these two distinct cases.

We first explore an event, recorded in airglow and wind data taken at Bear Lake Observatory (42 deg. N latitude, 111 deg. W longitude), where a wave of tidal-scale provides a ducting region for a small-scale (22 km), fast (80 m/s) gravity wave. Using measured data along with analytical and numerical models, we examine the event and its prominent features. This wave is not significantly affected by background wind time-dynamics, and thus strongly resembles ducted waves reported by Isler et al. [1997]. It shares some features with a wave reported by Taylor et al. [GRL, 22, 2849, 1995], including a phase reversal between OH and OI emissions intensities [e.g., Snively and Pasko, GRL, 32(8), L08808, 2005, and references cited therein].

We next investigate hypothetical cases where the temporal and spatial dependencies of the duct may affect small-scale ducted wave propagation. Waves with scales on the order of several hundred kilometers, and periods on the order of a few hours or many tens of minutes, may support Doppler ducted wave propagation, albeit in a somewhat transient manner. For such ducts, the effects of duct dynamics may become easily observable over reasonable time scales, and manifest in ducted wave behavior due to the temporal and spatial dependence of the large-scale wave supporting the duct. These effects, and possible implications for observation, are explored analytically and numerically.

3.9 GWV.09: Winter mesospheric temperature inversion and tidal-gravity wave interactions – by Li, Tao

Status of First Author: Student NOT in the poster competition PhD

Authors: Tao Li Department of Physics Colorado State University taoli@lamar.colostate.edu
 Hanli Liu High Altitude Observatory National Center for Atmospheric Research liuh@ucar.edu
 Tao Yuan Department of Physics Colorado State University titus@lamar.colostate.edu
 Philip Acott Department of Physics Colorado State University acott@lamar.colostate.edu
 David Krueger Department of Physics Colorado State University krueger@lamar.colostate.edu
 Chiao-Yao She Department of Physics Colorado State University joeshe@lamar.colostate.edu

Abstract: On the night of December 02/03, 2004, the CSU sodium lidar system observed a temperature inversion starting from the beginning of the night at 85-90km with increasing amplitude in time and finally became a huge bulge at about 09:30UT extending from 80km to 100km. At the same time, both zonal wind and meridional wind above 90km increase dramatically as well as the wind shears. After 09:30UT, the temperature inversion starts to move downward with a speed that is comparable to the downward phase speed of the diurnal tide. The analysis on tidal day-to-day variability shows that diurnal amplitude of temperature has a dramatic change from one day to another with a strong increase when the temperature inversion is observed. Further analysis shows the dynamic instability also developed on the top of the temperature inversion at 09:30UT and 10:30UT due to a near adiabatic lapse rate and a strong vertical shear of the horizontal wind. When a gravity wave propagates into this unstable region near 95km, it tends to break, causing strong wind gradients and cooling above and warming below. Detailed studies are under way.

3.10 GWV.10: Climatology of Small-Scale Mesospheric Gravity Waves Observed over Antarctica – by Nielsen, Kim

Status of First Author: CEDAR student in the poster competition PhD

Authors: K. Nielsen, M.J. Taylor, Center for Atmospheric and Space Sciences (CASS), Physics Department, Utah State University, and M.J. Jarvis, British Antarctic Survey (BAS)

Abstract: As part of a collaborative research program between the British Antarctic Survey and Utah State University an all-sky CCD imager was deployed in Antarctica to investigate the occurrence and properties of short-period (≈ 1 hour) mesospheric gravity waves at high latitudes. The measurements were made from two sites: Halley Station (75.5S, 26.7W), and Rothera Research Station (67.3 S, 68.1 W) to help investigate differences in wave propagation characteristics associated with mountain wave generation over the Antarctic peninsula (as observed from Rothera). Observations were made over five consecutive winter seasons from 2000-2003 (two seasons from Halley Station and two from Rothera). In this study we have analyzed the spatial and temporal properties of over 300 spatially extensive, short-period gravity wave events observed in the NIR OH emission (altitude ≈ 87 km). Our results show significant anisotropy in the gravity wave propagation headings observed from both sites suggesting a dominant poleward component for the wave propagation headings ($\approx 80^\circ$)

3.11 GWV.11: A curved gravity wave in the mesospheric airglow images – by Suzuki, Shin

Status of First Author: CEDAR student in the poster competition PhD

Authors: Shin Suzuki (Solar-Terrestrial Environment Laboratory, Nagoya University, shin@stelab.nagoya-u.ac.jp), Kazuo Shiokawa (Solar-Terrestrial Environment Laboratory, Nagoya University, shiokawa@stelab.nagoya-u.ac.jp), Yuichi Otsuka (Solar-Terrestrial Environment Laboratory, Nagoya University, otsuka@stelab.nagoya-u.ac.jp), Tadahiko Ogawa (Solar-Terrestrial Environment Laboratory, Nagoya University, ogawa@stelab.nagoya-u.ac.jp), Kenji Nakamura (Hydrospheric Atmospheric Research Center, Nagoya University), Takuji Nakamura (Research Institute for Sustainable Humanosphere, Kyoto University) **Abstract:** We found a unique wave structure, which had arc-like curved wave fronts in high contrast, by using an all-sky airglow imager located at Shigaraki (34.9N, 136.1E) on October 3, 2002. The curved structure was identified over 2.5 hours (1330-1600 UT: 2230-0100 LT) both in the OI (557.7 nm) and OH-band (720-910 nm) images. The wave structure had a wavelength of about 35 km and propagated concentrically northeastward with a horizontal phase velocity of about 80 m/s. The wave had a high frequency of 0.02 rad/s and had a momentum flux of 2.2 (m/s)^2 . Assuming that the wave pattern originated from a point source in the troposphere, the center of the curvature was projected on the sea near the Shikoku island, Japan, where developing cumulonimbus were recognized by the GMS-5 satellite and in the precipitation radar images.

3.12 GWV.12: Gravity Waves Activity over Brazil Inferred from CHAMP GPS-RO Temperature Profiles – by Wrasse, Cristiano

Status of First Author: Nonstudent

Authors: Wrasse, C.M.(cmw@laser.inpe.br)¹ Fechine, J.(joaquim@laser.inpe.br)¹ Takahashi, H.(hisaotak@laser.inpe.br)¹ Medeiros, A.F.(afragoso@df.ufcg.edu.br)² Wickert, J.(jens.wickert@gfz-potsdam.de)³

1. Instituto Nacional de Pesquisas Espaciais (INPE), Brazil

2. Universidade Federal de Campina Grande, Brazil

3. The German Research Center for Earth Sciences, GFZ, Germany

Abstract: Stratospheric gravity wave activities are deduced from GPS radio occultation temperature profiles obtained by CHAMP satellite. Potential energy profiles are used to analyze the gravity wave activity, seasonal variability and possible wave sources. Mesospheric gravity wave observations, using all sky imager, are compared with the stratospheric potential energy in order to investigate the gravity wave occurrence. The results show that the gravity wave activity over Brazil is strongly correlated with mesoscale synoptics systems that produce deep convection, such as mesoscale convective systems, squall lines, cold fronts and the Intertropical Convergence Zone.

3.13 GWV.13: The sodium signature of an overturning gravity wave – by Xu, Jiyao presented by Smith, Anne

Status of First Author: Nonstudent

Authors: Jiyao Xu, Chinese Academy of Science (xujy@center.cssar.ac.cn); Anne K. Smith, NCAR (aksmith@ucar.edu); Richard L. Collins, University of Alaska (rlc@gi.alaska.edu); Chiao-Yao She, Colorado State University (joeshe@lamar.colostate.edu)

Abstract: We present theoretical results and observations showing the evolution of the sodium layer in the presence of an overturning gravity wave. A time-dependent, nonlinear, photochemical-dynamical gravity wave model of the sodium layer indicates that the mixing ratio of atomic sodium is a very good tracer for the overturning of the gravity wave. However, the sodium number density perturbation has a behavior that is significantly different from that of temperature. At the bottomside of the sodium layer, a gravity wave with a small vertical scale of 10 km can lead to overturning in the sodium density even when the wave is stable. On the other hand, a gravity wave with a large vertical scale of 30 km does not lead to overturning of the sodium density structure even when the gravity wave itself is breaking. The evolution of the sodium mixing ratio gives a reliable determination of the overturning of the gravity wave. We present lidar observations of several overturning signatures in the sodium layer. These observations are part of a 14-day set of sodium density, temperature and wind measurements made with the Colorado State University sodium lidar in September 2003. We also derive potential temperature and sodium mixing ratio from the lidar data under the assumption of hydrostatic equilibrium. We compare the observed sodium density signatures with the evolution of temperature, potential temperature and mixing ratio. We discuss the lidar observations in terms of the model results.

3.14 GWV.14: Numerical Simulations of Upward Propagating Gravity Waves in the Middle Atmosphere – by Yu, Yonghui

Status of First Author: Student NOT in the poster competition PhD

Authors: Yonghui Yu Embry-Riddle Aeronautical University University of Central Florida
Yonghui.Yu@erau.edu
Michael P. Hickey Embry-Riddle Aeronautical University Michael.Hickey@erau.edu

Abstract: A time-dependent numerical model is described that solves the Navier-Stokes equations in two spatial dimensions to evaluate the characteristics of gravity waves generated in the lower atmosphere that propagate up through the middle atmosphere. Starting from the linear case in an initially motionless, isothermal and adiabatic atmosphere the model produces fluctuations in density, pressure and velocity that agree with basic theory. Based on the simulation results obtained including viscous effects a brief analysis of the forcing effects of the waves on the mean state of the upper atmosphere is presented. Finally, future numerical studies of nonlinear effects are described.

3.15 GWV.15: Evolution of a Mesospheric Bore Wave using 2D Local Spectral Analysis – by Stockwell, R.

Status of First Author: Nonstudent PhD

Authors: R.G. Stockwell Colorado Research Associates Division, Northwest Research Associates Inc., 3380 Mitchell Lane, Boulder, CO 80301. (stockwell@co-ra.com)
M.J. Taylor, and K. Nielsen, Center for Atmospheric and Space Sciences, Utah State University, Logan, Utah, USA
M. Jarvis, British Antarctic Survey, Cambridge, U.K.

Abstract: All-sky CCD observations of mesospheric gravity waves have been made from Halley Station Antarctica (75.5 S, 26.7 W) as part of a collaborative research program between British Antarctic Survey,

U.K. and Utah State University, USA. An unusual mesospheric bore event was observed in the OH nightglow emission (87 km) over a period of approximately hours on 27 May, 2001. A two dimensional localized spectral analysis is employed to reveal the time evolution of the bore wave packet. The nature of the local spectral analysis allows one to measure the characteristics of the wave packet (such as the wavenumber and phase speed) as a function of space (x,y) and time (t). In doing so, the evolution of the bore wave packet can be described. This Antarctic event is characterized by an extensive, high contrast linear wave front. The individual wave crests exhibited a spatially localized acceleration, possibly due to a sudden change in depth of the duct. Also, during this period of wave acceleration, the horizontal wavelength decreases during the period of wave acceleration from approximately 25 km to 18 km.

4 Other Wave Studies

4.1 OWV.01: Planetary Wave Calculations using the Global Scale Wave Model (GSWM) – by Stockwell, R.

Status of First Author: Nonstudent PhD

Authors: R.G. Stockwell Colorado Research Associates Division, Northwest Research Associates Inc., 3380 Mitchell Lane, Boulder, CO 80301. (stockwell@co-ra.com)

Abstract: The Global Scale Wave Model has been employed here to study vertically propagating planetary waves from the troposphere to the mesosphere and thermosphere. This has resulted of the creation of a large data set of GSWM Planetary Wave realizations which are publically available on the WWW at www.cora.nwra.com/gswm. These calculations have been processed for various wind models, zonal wavenumbers, period (from 1 to 30 days) and month of the year, resulting in a global (latitude vs height) map of planetary wave data. The GSWM resultant data fields are: 1) zonal wind amplitude and phase 2) meridional wind amplitude and phase 3) vertical wind amplitude and phase 4) temperature amplitude and phase. A summary of these results will be presented.

4.2 OWV.02: The 8-Hour Tide in the Mesosphere and Lower Thermosphere over the UK, 1988 - 2004 – by Beldon, Charlotte

Status of First Author: CEDAR student in the poster competition PhD

Authors: C.L.Beldon and N.J.Mitchell **Abstract:** Horizontal winds in the mesosphere and lower thermosphere have been measured by a VHF meteor radar in Castle Eaton, UK (52.6N, 2.2W). The measurements span the 16-year interval from January 1988 to January 2004. The complete data set has been used to investigate the 8-hour (terdiurnal) tide which at this latitude appears as a persistent feature of the atmosphere. Instantaneous amplitudes can be as large as 25 ms⁻¹. However, the monthly-mean values are smaller and range from 1 ms⁻¹ to 5 ms⁻¹. A clear seasonal behaviour is evident, in which the largest amplitudes are observed in autumn and early winter (September–November) and the smallest amplitudes are observed in early summer (May). In general, the phase difference between the zonal and meridional components is close to 2 hours, indicating a circularly polarised motion. Conspicuous inter-annual variability is seen in both the amplitude and phase. The amplitude of the tide sometime exhibits a day-to-day periodic modulation at frequencies associated with planetary waves (particularly the 2-day wave), indicating a degree of non-linear coupling between the tide and planetary waves.

4.3 OWV.03: Arctic mesopause region dynamics during the Stratospheric Polar Vortex season – by Bhattacharya, Yajnavalkya

Status of First Author: CEDAR student in the poster competition PhD

Authors: Yajnavalkya Bhattacharya, yajnaval@yorku.ca Gordon Shepherd gordon@yorku.ca

Abstract: Mesopause region winds from two emission layers - the hydroxyl Meinel band and atomic oxygen green line were measured using a Michelson Interferometer stationed at Resolute Bay, Canada (74 deg N). The measured winds are investigated for tidal, planetary and gravity wave signatures. An attempt is made to distinguish between propagating and non-propagating waves. Observations are compared to model simulations, e.g. with the TIME-GCM.

4.4 OWV.04: Mean Structure and Variability of the Diurnal Tide in the NCAR Whole Atmosphere Community Climate Model – by Chang, Loren

Status of First Author: CEDAR student in the poster competition Masters

Authors: Loren Chang University of Colorado, Department of Aerospace Engineering Sciences, Boulder CO changlc@colorado.edu
 Scott Palo University of Colorado, Department of Aerospace Engineering Sciences, Boulder CO scott.palo@colorado.edu
 Maura Hagan National Center for Atmospheric Research, Boulder CO hagan@ucar.edu
 Jadwiga Beres National Center for Atmospheric Research, Boulder CO beres@ucar.edu
 Rolando Garcia National Center for Atmospheric Research, Boulder CO rgarcia@ucar.edu

Abstract: The Whole Atmosphere Community Climate Model (WACCM) is a General Circulation Model (GCM) developed at NCAR using components from three well-validated atmospheric models. The dynamics core model is taken from the NCAR Middle Atmosphere Community Climate Model (MACCM), the chemistry and related processes are taken from the Model for OZone And Related chemical Tracers (MOZART), and additional chemical and physical processes needed to represent the Mesosphere and Thermosphere are taken from the Thermosphere Ionosphere Mesosphere Electrodynamics General Circulation Model (TIME-GCM). The dynamical framework of WACCM is derived from MACCM, a GCM that extends from the ground to 85 km. The dynamical governing equation is solved with a semi-Lagrangian technique at T63 horizontal resolution. In the upper mesosphere and above, additional processes such as molecular viscosity and auroral heating must be included; the formulations for these processes are taken from the TIME-GCM model. Important mesospheric and lower-thermospheric dynamical features such as the atmospheric tides and global scale planetary waves are excited self consistently in the model and are free to interact.

The goal of our research is to understand the relative importance of nonlinear interaction with large-scale planetary waves in the temporal and spatial evolution of the atmospheric tides. To this end we begin by investigating the monthly mean migrating diurnal tidal structure and the daily variability of the diurnal tide about the monthly mean in an effort to validate the diurnal tidal structure in WACCM. For these comparisons we have started with model runs from version 2 of WACCM for the months of January and July. The monthly mean values are first compared with the Global Scale Wave Model (GSWM) which has undergone extensive comparisons with mesospheric and lower-thermospheric wind and temperature observations. The dominant features of the diurnal tide, such as maximum amplitudes in the lower-thermosphere tropics for the wind field and the equator for the temperature field are consistent with classical tidal theory and the GSWM as expected. However, the absolute tidal amplitudes, height of maximum amplitude and hemispheric asymmetry are all significantly different between the models. Because the GSWM is a linear mechanistic model, we can only assess the linear processes such as water vapor heating, mean wind structure and dissipation. These fields are extracted from WACCM and compared with the GSWM to understand the reason for the differences. Tidal variability for January and July are calculated and will be presented.

4.5 OWV.05: Observations of Lunar Tides in the Mesosphere and Lower Thermosphere at Arctic and Middle Latitudes – by Sandford, David

Status of First Author: CEDAR student in the poster competition PhD

Authors: D. J. Sandford, N. J. Mitchell
 Department of Electronic and Electrical Engineering, University of Bath, Bath, BA2 7AY, UK
 D.J.Sandford@bath.ac.uk N.J.Mitchell@bath.ac.uk

Abstract: Meteor radars have been used to measure the horizontal winds in the mesosphere and lower thermosphere over Castle Eaton (52N) in the UK and over Esrange (68N) in Arctic Sweden. The signature of the lunar (M2) tide has been identified at both locations and can reach amplitudes as large as 11ms⁻¹. We consider a 16-year data set covering the interval 1988 - 2004 for the UK and a 5-year data set covering the interval 1999 - 2004 for the Arctic. The Arctic radar has an interferometer and so allows investigation of the vertical structure of the lunar tide. At both locations the tide has maximum amplitudes in winter. The amplitude is found to increase with height over the 80 - 100 km height range observed. Vertical wavelengths are very variable, ranging from about 15 km in summer to more than 70km in winter. The decadal-scale variability of the mid-latitude lunar tide is quantified.

4.6 OWV.06: A Climatology of Tidal Temperatures from TIMED/SABER – by Zhang, Xiaoli presented by Zhang, Xiaoli

Status of First Author: Student NOT in the poster competition PhD

Authors: Xiaoli Zhang, Jeffrey M. Forbes, Scott E. Palo Department of Aerospace Engineering Sciences,
University of Colorado, Boulder, CO

Maura E. Hagan High Altitude Observatory, NCAR, Boulder, CO

Saburo Miyahara Department of Earth and Planetary Sciences, Kyushu University, Fukuoka, Japan

J. Russell Center for Atmospheric Sciences, Hampton University, Hampton, VA

C.J. Mertens and M.G. Mlynczak NASA Langley Research Center, Hampton, VA

Abstract: The SABER instrument on TIMED provides unprecedented geographical coverage for the determination and study of atmospheric tides. However, the slow local time precession rate of TIMED can cause longer-term temperature variations to alias into the tidal signals. A new method of analyzing satellite temperature data for tides has been developed to circumvent this difficulty, but at the expense of temporal resolution of the tidal fields, i.e., 120-day mean tidal structures are obtained. In this work, we apply this method to derive a series of 120-day mean tidal structures, extending between 80-120 km altitude, 50S - 50N latitude, and centered on each month from September 2003 to September 2004. Besides the migrating diurnal and semidiurnal tides, the eastward-propagating diurnal tide with zonal wavenumber 3 (DE3) is found to dominate the tidal temperature fields in this geographical region. The abilities of the Global-Scale Wave Model and the Kyushu University General Circulation Model to approximate the observed tidal fields are also assessed.

5 Lidar Studies

5.1 LID.01: Lidar Observations of Gravity Wave Spectra at Arecibo – by Hassiotis, Alexander

Status of First Author: CEDAR student in the poster competition PhD

Authors: Alexander Hassiotis, Pennsylvania State University (PSU), adh180@psu.edu Dr. Jonathan S. Friedman, Arecibo Observatory, jonathan@naic.edu Dr. Tim Kane, PSU, tjk7@psu.edu

Abstract: Resonance lidar measurements of potassium densities in the altitude range 82-105 km have been taken at the Arecibo observatory (18N,67W) since July 1999. Gravity wave parameters are extracted from the density fluctuations and a statistical analysis is performed.

5.2 LID.02: Comparison of Meteor Radar Wind Measurements at Barrow and Dixon Island – by Iimura, Hiroyuki

Status of First Author: CEDAR student in the poster competition PhD

Authors: Hiroyuki Iimura. University of Colorado at Boulder, USA. iimurah@colorado.edu. Scott E. Palo. University of Colorado at Boulder, USA. palo@colorado.edu. Nikolai A. Makarov. Institute for Experimental Meteorology, Obninsk, Russia. makarov@typhoon.obninsk.ru

Abstract: Meteor radar systems measure line-of-sight wind velocities from Doppler frequencies in radar signals reflected back from meteor trails. Because the meteor trails occur at an altitude region between 70 and 100 km, the horizontal wind velocities in the mesosphere and lower-thermosphere regions can be measured by the meteor radar systems. To observe the wind fields of the mesosphere and lower-thermosphere over the Arctic and Antarctic regions, the University of Colorado at Boulder, USA and the Institute for Experimental Meteorology in Obninsk, Russia have installed meteor radar systems in the northern and southern polar regions. In the northern polar region, two meteor radar systems are located at Barrow Alaska (71.3N, 156.8W), USA and Dixon Island (73.5N, 80.6E), Russia. The meteor radar system at Barrow was initially installed in July 2001 and has operated continuously from July 2002 to October 2004. The Barrow meteor radar system operates at a frequency of 46.3 MHz and utilizes four 6-element Yagi antennas for the signal transmission and reception. The meteor radar system at the Dixon Island was installed in September 1999. The the Dixon Island meteor radar system has operated at a frequency of 33.6 MHz and utilizes four 5-elements Yagi antennas for the signal transmission and reception. These two meteor radar systems measure the horizontal wind velocities along the four cardinal geographic directions. With observations from the Arctic in both the Russian and north American hemispheres we will utilize our measurements to investigate the large scale wave structure in the Arctic mesosphere and lower-thermosphere. Estimates for the atmospheric tidal amplitudes and phases in addition to long period planetary waves will be determined and intercompared. These observations will also be compared with the global scale wave model to provide a global context for the observations. When coincident measurements are available we will make an effort to separate migrating from stationary features to quantify the degree of longitudinal variability present at high latitudes.

5.3 LID.03: Observations and Modeling of Mesospheric Potassium Layer over the Arecibo Observatory – by Ruben, Delgado

Status of First Author: CEDAR student in the poster competition PhD

Authors: Ruben Delgado(rdeldgado@naic.edu)-Univ. of Puerto Rico; Brad R. Weiner(brad@hpcf.upr.edu)-Univ. of Puerto Rico; Jonathan S. Friedman(jonathan@naic.edu)-NAIC Arecibo Observatory

Abstract: Nighttime observations of the atmospheric potassium layer were performed at the Arecibo Observatory using lidar to determine the seasonal variation in the concentration of the metal atom layer. The K layer shows nightly and seasonal variation; the nightly variation was due to

the presence of sporadic layers. The seasonal variability is less in the layer width, while the column abundance exhibits a semiannual variation. To identify possible molecular reservoirs and sinks in the K layer, ab initio calculations were performed to estimate the thermochemistry. Rate constants for ion-molecule reactions, were obtained by considering Langevin theory, constrained by a detailed balance mechanism. Reactions $\text{KO}^+ + \text{N}_2$, $\text{KO}_2^+ + \text{O}$, $\text{KO}_2^+ + \text{N}_2$, and $\text{KHCO}_3 + \text{H}$ can be considered as routes that may cycle species, which can play a role as major sinks of potassium ion or neutrals in the mesospheric cycle. To understand the mesospheric K layer a one dimensional model was developed. The model includes a meteoric deposition, vertical transport through eddy diffusion, and a full chemical scheme. The predominant potassium species is KHCO_3 as a result of the influence of odd oxygen/hydrogen chemistry. The study of the metal layer contributes to a better understanding of chemical and dynamic changes that affect atmospheric composition.

5.4 LID.04: Analysis of Wind Speed and Wind Shear Statistics and Small Scale Structure using Doppler Lidar Data from New Mexico and Hawaii – by Zhou, Xiaoqian

Status of First Author: Student NOT in the poster competition PhD

Authors: X. Zhou and M. F. Larsen, Department of Physics, Clemson University, Clemson, South Carolina **Abstract:** We present an analysis of the statistical distribution of the wind speeds and vertical wind shears in the upper mesosphere and lower thermosphere by using Doppler Sodium lidar data from the Starfire lidar in New Mexico and from the Maui/MALT lidar in Hawaii. Here, we focus on the distribution of wind speed and shear magnitude as a function of height in the altitude range from 75 km to 105 km. A similar analysis was carried out by Larsen (JGR, 2002) for an extensive set of midlatitude rocket chemical release wind measurements in the altitude range from 90 to 140 km. The overlap in the height range coverage by the lidar and rocket measurements allows us to compare the results directly, at least in the region where the height coverage overlaps. In addition, the lidar data set extends the altitude coverage for the analysis below 90 or 95 km where the available chemical release data is much more limited. The results indicate a general decrease in the maximum wind speeds with height below the altitude of the maximum found in the earlier study, but the wind speeds are still generally larger and have larger shears than would be expected from tidal theory or general circulation model predictions.

6 Stratosphere Studies and Below

6.1 SSB.01: Polar stratospheric clouds observed by a lidar at Rothera, Antarctica – by Simpson, Shawn

Status of First Author: CEDAR student in the poster competition Undergraduate

Authors: Shawn E. Simpson, Xinzhao Chu, Alan Z. Liu Department of Electrical and Computer Engineering University of Illinois at Urbana-Champaign 1308 West Main Street, Urbana, IL 61801, USA Email: simpson1@uiuc.edu, xchu@uiuc.edu, liuzr@uiuc.edu
Graeme J. Nott, Jan Diettrich, Patrick J. Espy Physical Science Division British Antarctic Survey High Cross, Madingley Road, Cambridge, CB3 0ET, UK Email: GNO@south.nerc-bas.ac.uk, jadi@bas.ac.uk, PJE@bas.ac.uk

Abstract: The University of Illinois iron Boltzmann temperature lidar was installed at the British Antarctic Survey station (Rothera, 67.5S, 68.0W) on the Adelaide Island near the Antarctic Circle in December 2002, and has been operated there for over 2 years. Previously, this lidar was deployed at the US Amundsen-Scott South Pole Station (90S) from November 1999 to October 2001 for 2 years. This lidar operates at two UV wavelengths of 372 and 374 nm, and can measure temperature in the middle and upper atmosphere, Fe density, polar mesospheric clouds (PMC) and polar stratospheric clouds (PSC). Here we report the PSC data collected in the winters of 2003 and 2004 at Rothera, and compare them with the PSC data collected at the South Pole in the winters of 2000 and 2001. The altitude, layer width and structure, peak backscatter coefficient of PSC and their seasonal variations will be characterized using the lidar data. Balloon radiosonde data will be used to investigate the temperature and wind structures in the presence of PSC. As we know, this is the first characterization of PSC by a lidar at Rothera Station.

6.2 SSB.02: Study of the Temperature Structure of the Middle Arctic Atmosphere – by Thurairajah, Brentha

Status of First Author: CEDAR student in the poster competition PhD

Authors: Brentha Thurairajah (ftbt@uaf.edu), Sharma Nadakuditi (ftbn@uaf.edu), and Richard Collins (rlc@gi.alaska.edu): University of Alaska, Fairbanks, Alaska **Abstract:** Recent studies of the stratosphere and mesosphere (middle atmosphere), and the troposphere (lower atmosphere) indicate that the structure of the stratospheric vortex is correlated with variations in the Arctic Oscillation (AO). The circulation of the Arctic stratospheric vortex is also coupled with the circulation of the Aleutian High Pressure System (the Aleutian High). A Rayleigh lidar system has been operated at Poker Flat Research Range, Chatanika, Alaska (65N, 147W) since 1997. The seven-year lidar measurements provide middle atmosphere temperature profiles (40–80 km). From this data set the variability of the middle atmosphere temperature structure from year-to-year has been examined. A comparison of these temperature profiles with MSIS data, and UKMO synoptic maps of wind and geopotential height is presented. This comparison can be used to correlate changes in vertical temperature profile with changes in the Aleutian High and the stratospheric vortex. This analysis will provide the foundation for the proposed observational and modeling study of the Arctic stratosphere and mesosphere during the International Polar Year (IPY).

7 Sprite and Terrestrial Gamma-ray Flash (TGF) Studies

7.1 SPR.01: On the OH nightglow emission at Sprite temperatures in the MLT region – by Fritz, Jason

Status of First Author: CEDAR student in the poster competition Undergraduate

Authors: Jason Fritz Penn State Lehigh Valley jsf186@psu.edu
Tai-Yin Huang Penn State Lehigh Valley tuh4@psu.edu

Abstract: Recent observations on sprites have revealed that the temperature in the intense discharge channels above thundercloud tops in the mesosphere could be as high as 20,000 K or above. Sprites are usually associated with positive cloud-to-ground (+CG) strokes of lightning. They are transient luminous flashes, each lasts a few to tens of milliseconds. Because some chemical reaction rates are highly dependent on temperatures, it is speculated that sprites should have a significant effect on chemistry. This study is aimed to investigate how OH nightglow emission in the MLT region is affected when sprites occur at a temperature of 20,000 K during successive transient flashes. Our model simulation results, ignoring dynamical effects, indicate a huge loss of O₃ and OH occurring between 75 km and 90 km, leaving little doubt about the significant role of sprites on chemistry in the MLT region.

7.2 SPR.02: Testing Sprite Initiation Theories Using Lightning Measurements and Modeled EM Fields – by Hu, Wenyi presented by Hu, Wenyi

Status of First Author: CEDAR student in the poster competition PhD

Authors: Wenyi Hu, Duke University, wyhu@ee.duke.edu
Steven A. Cummer, Duke University, cummer@ee.duke.edu
Walter A. Lyons, FMA Research Inc., walyons@frii.com

Abstract: Combining the optical observation and sferic measurement data, we tested the existing theories of sprite initiation rigorously by comparing the measurement data, the numerical model predictions and theoretical threshold quantitatively. We selected for this analysis a set of sprite events from the summers of 2004 with high signal-to-noise ratio (SNR) and well-bounded sprite initiation time from experimental data. Then we measured the current moments and charge moment changes from the recorded magnetic fields radiated by the causative lightning strokes. The measured current moments are then used as the input of our 2-D cylindrical full wave numerical model for lightning-generated EM fields. We compare the simulated mesospheric electric fields to the theoretical threshold electric field for conventional breakdown. After analyzing various species of sprite events, we find the required mesospheric electric field for sprite initiation might be lower than the threshold for conventional breakdown. The intensity of the optical emission is related to the mesospheric electric field at the sprite initiation time. Also, we found long-delayed sprites caused by intense continuing current usually occur at lower altitudes and are more likely to be associated with sprite currents. The charge moment change for sprite initiation derived through this method is generally consistent with previous statistical research results but its range is further narrowed down in this work.

7.3 SPR.03: Using WWLLN to provide insight on Terrestrial Gamma Ray Flashes – by Lay, Erin

Status of First Author: CEDAR student in the poster competition PhD

Authors: Erin H. Lay, Robert H. Holzworth, Craig J. Rodger, Abram Jacobson, Liliana Lopez, and David Smith
Abstract: The World Wide Lightning Location Network (WWLLN) provides real time lightning locations globally by measuring the very low frequency (VLF) radiation emanating from lightning discharges. We use this real time global lightning data to provide insight on terrestrial gamma ray flashes (TGFs) measured by the RHESSI spacecraft. Comparison of TGFs to WWLLN lightning data indicate that TGFs are linked to lightning globally. WWLLN lightning flashes closely linked in time and space to TGF events indicate that larger lightning strokes could play a role in generating TGFs.

7.4 SPR.04: Comparison of Results from Sprite Streamer Modeling with Spectrophotometric Measurements by ISUAL Instrument on FORMOSAT-2 Satellite – by Liu, Ningyu presented by Liu, Ningyu

Status of First Author: CEDAR student in the poster competition PhD

Authors: Ningyu Liu¹, Victor Pasko¹, Harald Frey², Stephen Mende², Han-Tzong Su³, Alfred Chen³, Rue-Ron Hsu³, Lou-Chuang Lee^{3,4}, Hiroshi Fukunishi⁵, and Yukihiro Takahashi⁵

¹ The Pennsylvania State University, Communications and Space Sciences Laboratory, University Park, PA 16802, USA ² University of California at Berkeley, Space Sciences Laboratory, Berkeley, CA 94720, USA ³ National Cheng Kung University, Physics Department, Tainan 70101, Taiwan ⁴ National Applied Research Laboratories, Taipei 106, Taiwan ⁵ Tohoku University, Department of Geophysics, Sendai 980-8578, Japan

Abstract: Sprites commonly consist of large numbers of needle-shaped filaments of ionization [e.g., Gerken and Inan, JASTP, 65, 567, 2003] and typically initiate at altitudes 70-75 km in a form of upward and downward propagating streamers [Stanley et al., GRL, 26, 3201, 1999; Stenbaek-Nielsen et al., GRL, 27, 3829, 2000; McHarg et al., JGR, 107, 1364, 2002; Moudry et al., JASTP, 65, 509, 2003]. A two-dimensional model has been recently developed at Penn State for studies of dynamics of positive and negative streamers for a wide range of air pressures under the influence of external electric fields of various strength, and the corresponding modeling results on characteristics of sprite streamers and their optical and UV emissions have been reported in [Liu and Pasko, JGR, 109, A04301, 2004; GRL, in press, 2005]. Modeling results on optical and near-UV emissions of sprite streamers [Liu and Pasko, 2004] agree with the sprite observations demonstrating domination of red emissions in the sprite spectrum [e.g., Mende et al., 1995; Hampton et al., 1996] and presence of short bursts of blue emissions at the formation stage of sprites [e.g., Armstrong et al., JASTP, 60, 787, 1998; Suszcynsky et al., JASTP, 60, 801, 1998]. The modeling studies of far-UV emissions of sprite streamers due to N₂ LBH band system indicate that these emissions at 70 km are generally stronger by a factor of 10 than those from the first negative band system of N₂⁺ [Liu and Pasko, 2005]. The recent successful launch of the ISUAL instrument on FORMOSAT-2 satellite [Chern et al., JASTP, 65, 647, 2003] provides new opportunities for studies of sprite spatial, temporal and spectral properties from a global point of view. The ISUAL instrument contains a spectrophotometer with six individual photometers covering the spectral range from the far ultraviolet to the near infrared. Observational results on time-resolved spectral signatures of sprites obtained by ISUAL instrument have been recently reported in [Mende et al., Eos Trans. AGU, 85(47), Fall Meet. Suppl., Abstract AE51A-02, 2004; Frey et al., Eos Trans. AGU, 85(47), Fall Meet. Suppl., Abstract AE51A-05, 2004]. One of the most important results of the spectral measurements by ISUAL instrument is the detection of the far-UV emissions from sprites [e.g., Frey et al., 2004], which are not observable by the ground and aircraft based instruments due to the strong absorption by atmospheric O₂. In this talk, we will present modeling results on emissions from sprite streamers and compare them with a few selected observations obtained by the ISUAL spectrophotometer. The comparison will focus on the intensity ratios of four different emissions, which include N₂ Lyman-Birge-Hopfield band system, the first and second positive band systems of N₂, and the first negative band system of N₂⁺. The considered intensity ratios are useful for deriving the information about the energetics of the electrons in sprites from the experimental data.

7.5 SPR.05: Lightning-driven electric and magnetic fields measured in the stratosphere during the Brazil 2002-03 Balloon Campaign – by Thomas, Jeremy

Status of First Author: CEDAR student in the poster competition PhD

Authors: Jeremy N. Thomas (U. of Washington, jnt@u.washington.edu), Robert H. Holzworth (U. of Washington, bobholz@ess.washington.edu), Michael P. McCarthy (U. of Washington, mccarthy@ess.washington.edu), Osmar Pinto Jr. (INPE, Brazil, osmar@dge.inpe.br)

Abstract: During the Brazil Sprite Balloon Campaign 2002-2003, thousands of the lightning-driven electric and magnetic field changes were measured in the stratosphere above 30 km in altitude.

Two-hundred of these lightning events occurred within 75 km horizontal distance of the balloon payload and drove quasi-electrostatic field (QSF) changes of up to 140 V/m measured at the payload. The amplitude and relaxation time of these nearby lightning events generally agree with a numerical QSF model developed by the authors, thus verifying that lightning does indeed generate significant electric fields due to the redistribution of cloud charge above the thundercloud in the middle atmosphere. The balloon-borne data also suggests that positive cloud-to-ground (+CG) lightning and in-cloud (IC) lightning generally produce larger nearby electric field changes compared to negative cloud-to-ground lightning (-CG), which agrees with the correlation between large +CG strokes and sprites. Although the sprite imaging cameras were blocked by clouds during these balloon flights, these QSF can be predicted at sprite altitudes using the in situ data along with this numerical QSF model. It is found that the electric fields at sprite altitudes (60-90 km) never surpass breakdown when the fields for each of these 200 nearby lightning events are propagated to the mesosphere. In addition to measuring nearby electric fields, the balloon payloads measured thousands of ELF to VLF electric and magnetic fields from distant lightning (>75 km). These ELF to VLF fields generally agree with ground-based measurements [Cummer et al., GRL, 25, 1281, 1998] and models [Pasko et al., GRL, 25, 3493, 1998] but are in disagreement with the previous balloon-borne measurements during the Sprites99 Campaign [Bering, Adv. Space Res., 34, 1782, 2004]. The Brazil payloads measured ELF to VLF electric and magnetic field changes for every CG stroke at 75-600 km distance from the payload and rarely measured delayed ELF pulses after these CG spherics. The Sprites99 payloads rarely measured the CG spherics but for 90

7.6 SPR.06: 3D FDTD MODELING OF THE DIURNAL AND SEASONAL VARIATIONS IN SCHUMANN RESONANCE PARAMETERS – by Yang, Heng

Status of First Author: CEDAR student in the poster competition PhD

Authors: Heng Yang, Penn State University, hxy149@psu.edu Victor P. Pasko, Penn State University, vpasko@psu.edu

Abstract: Observations of Schumann resonances (SR) in the Earth-ionosphere cavity [Schumann, Z. Naturforsch., 7a, 149, 1952] represent a powerful tool for variety of remote sensing applications [e.g., Williams, Science, 256, 1184, 1992; Cummer, IEEE Trans. Antennas Propagat., 48, 1420, 2000; Roldugin et al., JGR, 109, A01216, 2004], which in recent years included studies of thunderstorm related transient luminous events in the middle atmosphere and related lightning discharges [e.g., Sato and Fukunishi, GRL, 30, 1859, 2003; Su et al., Nature, 423, 974, 2003]. The observed SR parameters are strongly related to the conductivity distributions and global lightning activity in the Earth-ionosphere cavity. In the realistic cavity, the conductivity distribution is not laterally uniform, but varies with the local time and seasons. Additionally, the lightning activity in the three main areas (Africa, South-East Asia, and South America) exhibits strong diurnal and seasonal variation patterns. The resultant diurnal and seasonal variability of the SR parameters has been well documented in the existing literature [e.g., Sentman and Fraser, JGR, 96, 15973, 1991; Satori, JATP, 58, 1483, 1996; Price and Melnikov, JASTP, 66, 1179, 2004]. In this talk we report results from a 3D FDTD model of the Earth-ionosphere cavity with realistic conductivity profile and realistic distribution of lightning sources, which is designed to account for the observed diurnal and seasonal variations of the SR parameters. The employed model was first introduced in [Yang and Pasko, EOS Trans. AGU, 84, Fall Meet. Suppl., AE42A-0796, 2003] and has recently been extensively validated [e.g., Yang and Pasko, GRL, 32, L03114, doi: 10. 1029/2004 GL021343, 2005] by comparisons of eigenfrequency and quality factor solutions derived from the model with a set of classical results available in the literature for the laterally uniform spherically symmetric Earth-ionosphere cavity [Sentman, JATP, 45, 55, 1983; JATP, 52, 35, 1990; JGR, 101, 9479, 1996; Greifinger and Greifinger, Radio Sci., 13, 831, 1978; Mushtak and Williams, JASTP, 64, 1989, 2002] and with the recent observations of SR during solar proton events and X-ray bursts [Roldugin et al., JGR, 106, 18555, 2001; JGR, 108, 1103, 2003; 2004]. In this talk, we will report comparisons of the FDTD model results with the diurnal and seasonal variability of SR parameters reported recently by Price and Melnikov [JASTP, 66, 1179, 2004]. The 3D FDTD model, which will be discussed in this talk, utilizes the International Reference Ionosphere [e.g., Bilitza, Radio Sci.,

36 (2), 261, 2001] to describe the realistic conductivity profile in the cavity corresponding to different local times and seasons. The diurnal variation of global lightning activity is adopted from [Sentman and Fraser, JGR, 96, 15973, 1991].

8 Coupling the Upper and Lower Atmosphere

8.1 CUL.01: DUMBO and the Ionosphere – by Livneh, Dorey

Status of First Author: CEDAR student in the poster competition PhD

Authors: Dorey J. Livneh, PSU, dull121@psu.edu John D. Mathews, PSU, jdmathews@psu.edu

Abstract: The Dual Microbarograph Observatory (DUMBO) consists of two microbarographs that are set up roughly 100 km apart, with one of the instruments located on the grounds of the Arecibo Observatory in Puerto Rico and the other at El Verde in the rain forest of eastern Puerto Rico. This configuration is used to detect the propagation and correlation properties of short periods (5 to 120 minutes) in barometric pressure features. Incoherent Scatter Radar data from Arecibo is used along with DUMBO to examine coupling between the ground level atmosphere and the ionosphere, especially during times of disturbance by major events such as hurricanes.

8.2 CUL.02: An Improved Approach for Atmosphere Data Analysis – by Zhang, Junbo presented by Zhou, Qihou

Status of First Author: CEDAR student in the poster competition Masters

Authors: Junbo, Zhang Miami University, zhangj3@muohio.edu
Matthew Timothy Brenneman, Miami University, brennemt@muohio.edu
Qihou, Zhou, Miami University, zhouq@muohio.edu

Abstract: This is an approach to analyze the energy distribution in the atmosphere data.

9 Meteor Science other than Winds

9.1 MET.01: Aeronomic Implications of Recent Arecibo UHF Meteor Observations – by Briczinski, S

Status of First Author: CEDAR student in the poster competition PhD

Authors: Stan Briczinski, Penn State, jsb144@psu.edu John Mathews, Penn State, jdmathews@psu.edu David Meisel, SUNY Geneseo, jmeisel@geneseo.edu

Abstract: The micrometeor observations performed using the 430 MHz Arecibo Observatory radar have proven to be crucial for the understanding of meteoric effects on the aeronomy of the upper atmosphere. A periodic FFT search algorithm has been used to automatically detect meteors during February of 2001 and April of 2004 between altitudes of 85 and 125 km. The February observations indicate the strong possibility of an observed shower originating from the Aten asteroid group. We show the parameters of the meteor 'micro shower' along with their orbital details. We assume a common composition for the shower elements, which explains their close statistical grouping not seen in sporadic events. We divide our meteors into two categories - those that possess a measurable deceleration and events that do not appear to decelerate. For the first class, we present the masses obtained from the decelerations. We compare the correlation of the $\ln(v^2/r)$ to height for decelerating and non decelerating categories. We propose that the deceleration may not be a necessary component for size and/or mass determinations. We also present the correlation techniques used to derive size distributions for non decelerating events. Finally, we propose the theory that all events in the microgram mass range (those events typically seen at Arecibo) undergo catastrophic destruction at the end of their lifetimes, i.e. all meteors observed at Arecibo behave as 'terminal events'.

9.2 MET.02: Calibration Issues in Meteor Radar Interferometers – by de la Pena, Santiago

Status of First Author: CEDAR student in the poster competition PhD

Authors: Santiago de la Pena CIRES delapena@ucsu.colorado.edu Elias Lau CIRES elias.lau@colorado.edu Susan Avery CIRES susan.avery@colorado.edu James Avery University of Colorado james.avery@colorado.edu

Abstract: Interferometry techniques for meteor radar applications have been in use around the world for several years. These techniques resolve the position of meteor trails, which yield better wind estimates and allow the analysis of meteor activity in a region. Several errors are introduced to the calculations due to antenna coupling, wrong spacing between antennas, differences in length between the different transmission lines, and the electronics in the receiver. We discuss the source of the errors and a methodology to solve for them.

9.3 MET.03: Mysteries of the MU - Initial Observations and Analysis of MU Meteor Data – by Malhotra, Akshay

Status of First Author: CEDAR student in the poster competition Masters

Authors: Akshay Malhotra, Penn State University, arm239@psu.edu John Mathews, Penn State University, JDMathews@psu.edu Qihou Zhou, Miami University of Ohio, zhouq@muohio.edu

Abstract: The MU radar with its capability to point perpendicular to the earth's magnetic field provides a unique opportunity to observe and study all three types of meteor echoes, namely classical trail-echoes, head-echoes and range spread trail-echoes simultaneously. The time and altitude distribution of these echoes during the pre and post-sunrise period provide some interesting results, particularly about the radio science issues surrounding range spread trail echoes. Some other interesting meteor-related observations are also shown along with their possible explanations. We present the distribution of all three kinds of events along with another possible subclass of events, the terminal events.

9.4 MET.04: Reconstructing classical meteor trail echoes a post-modern view – by Roy, Arnab

Status of First Author: CEDAR student in the poster competition PhD

Authors: Arnab Roy, Penn State University, aur112@psu.edu John F. Doherty, Penn State University, jfd6@psu.edu John D. Mathews, Penn State University, JDMathews@psu.edu

Abstract: Fresnel holography presents a powerful means of analyzing classical meteor trails. This technique is used to determine meteor speed for the Mu radar data. Moreover, we attempt to classify meteors echoes into different types based on unwrapped phase information of the return signal amplitude.

Index

- Abdo, Kevin, 13
Acott, P, 9
Azeem, Irfan, 11
- Bageston, Jose, 9
Beldon, Charlotte, 20
Beres, Jadwiga, 5
Bhattacharya, Yajnavalkya, 20
Briczinski, S, 31
Burrows, Susannah, 5
- Carlson, Chad, 13
Chang, Loren, 20
Chen, Meng-Yuan, 10
- de la Pena, Santiago, 31
- Fechine, Joaquim, 13
Fritz, Jason, 26
- Gobbi, Delano, 8, 9
Guo, Liyu, 5
- Hanner, Bonnie, 14
Harrell, Sean, 14
Hassiotis, Alexander, 23
Hoang, Thien, 14
Hu, Wenyi, 26
- Iimura, Hiroyuki, 23
- Kang, Chunmei, 10
Khanal, Harihar, 15
- Lay, Erin, 26
Li, Tao, 16
Liu, Ningyu, 27
Livneh, Dorey, 30
- Malhotra, Akshay, 31
- Nielsen, Kim, 16
Nozawa, Satonori, 6
- Oyama, Shin-ichiro, 6
- Reyes, Pablo, 10
Roy, Arnab, 32
Ruben, Delgado, 23
- Sandford, David, 21
Sharpee, Brian, 11
Simpson, Shawn, 25
- Slanger, Tom, 11
Smith, Anne, 18
Snively, Jonathan, 15
Stockwell, R., 18, 20
Suzuki, Shin, 17
- Thomas, Jeremy, 27
Thuraiajah, Brentha, 25
Tsuda, Takuo, 7
- Won, Y-I, 11
Won, Young-In, 7
Wrasse, Cristiano, 17
- Xu, Jiyao, 18
- Yang, Heng, 28
Yu, Yonghui, 18
Yue, Jia, 12
- Zhang, Junbo, 30
Zhang, Xiaoli, 22
Zhao, Yucheng, 7
Zhou, Qihou, 30
Zhou, Xiaoquian, 24